Gschnaller, Sandra

Working Paper

The albedo loss from the melting of the Greenland ice sheet and the social cost of carbon

ifo Working Paper, No. 332

Provided in Cooperation with:
Ifo Institute – Leibniz Institute for Economic Research at the University of Munich

Suggested Citation: Gschnaller, Sandra (2020) : The albedo loss from the melting of the Greenland ice sheet and the social cost of carbon, ifo Working Paper, No. 332, ifo Institute - Leibniz Institute for Economic Research at the University of Munich, Munich

This Version is available at:
https://hdl.handle.net/10419/222853

ifo WORKING PAPERS

332
2020

July 2020

The Albedo Loss from the Melting of the Greenland Ice Sheet and the Social Cost of Carbon

Sandra Gschnaller

ifo INSTITUTE

Leibniz Institute for Economic Research
at the University of Munich

Imprint:

ifo Working Papers
Publisher and distributor: ifo Institute – Leibniz Institute for Economic Research at the University of Munich
Poschingerstr. 5, 81679 Munich, Germany
Telephone +49(0)89 9224 0, Telefax +49(0)89 985369, email ifo@ifo.de
www.ifo.de

An electronic version of the paper may be downloaded from the ifo website:
www.ifo.de

ifo Working Paper No. 332

The Albedo Loss from the Melting of the Greenland Ice Sheet and the Social Cost of Carbon

Abstract

I extend the reduced Greenland ice sheet (GIS) model-module of DICE-GIS (Nordhaus, 2019) by integrating snow-albedo feedback (SAF) and potential tipping of the ice sheet into the resuming DICE-GIS SAF model. This novel model extension allows to quantify the social cost of carbon (SCC) more precisely because the economic damages are not only related to intensified sea level rise, but also an accelerated increase in global temperature. Accounting for the SAF raises the SCC from 274.92 to 319.67 $/t$CO_2$ in 2100, an increase of 16.3%. The temperature increase is the key channel through which the SAF impacts the SCC.

JEL Code: O13, Q15, Q58
Keywords: Social cost of carbon, climate change, Greenland ice sheet, snow albedo feedback, tipping

Sandra Gschnaller
ifo Institute – Leibniz Institute for
Economic Research
at the University of Munich
Poschingerstr. 5
81679 Munich, Germany
gschnallersandra@yahoo.de

1 Introduction

Snow-covered surfaces play an important role in the reflection of solar radiation and thus contribute to the temperature regulation of the planet. The interaction between snow and ice, and solar radiation is called snow-albedo feedback (SAF). The SAF cools the global climate. Snow- and ice-covered areas obtain a high albedo because they are highly reflective and, therefore, reflect a large amount of the incoming solar radiation. This cooling effect becomes particularly essential in light of climate change because it counteracts the rising temperature (Thackeray et al., 2019). However, the cooling effect has declined during the last decades, especially in the Arctic region due to the enhanced melting of snow and ice (Flanner et al., 2011). This, in turn, increases the risk of the irreversible melting of the Greenland ice sheet (GIS). I extend DICE-GIS (Nordhaus, 2019) by integrating SAF and potential tipping of the GIS to calculate the SCC more precisely, taking into account the reinforcing cycle between the change in the strength of the SAF, accelerated global warming, and the amplified hazard of tipping.

The fact that the GIS is melting more and more is not only alarming for the Arctic region but the whole planet. The melting of the entire GIS would result in a global sea level rise of about 7 m (IPCC, 2014; Bamber et al., 2013). This sea level rise is not restricted to future periods, it is already observable now. The mass loss of the GIS doubled from 2007 to 2016 relative to the previous decade (IPCC, 2019). Until 2100 the rise in global sea level due to the melting of the GIS is predicted to be 14 to 78 mm under the IPCC's conservative Representative Concentration Pathway 2.6 scenario with a limited mean temperature increase of 1.6°C until 2050 (Fürst et al., 2015; IPCC, 2014). Surface melting causes the major part of the volume loss of the GIS, while the actual discharge of ice plays a minor role (IPCC, 2019; Fürst et al., 2015; Helsen et al., 2017). Especially the intensity of summer melting sets new records at ever shorter intervals. Four records alone were set in the last decade in the years 2010, 2012, 2015, and 2019 (Tedesco et al., 2011, 2016b; Tedesco and Fettweis, 2019; Box et al., 2012; Nghiem et al., 2012).

Global warming not only leads to a decrease in the volume extent of the GIS, but also to a shrinking snow cover on top of it and thus to a loss of the surface area with the highest reflectivity, which refers to the so-called *darkening* of the GIS (Tedesco et al., 2016a). Besides, various processes decrease the reflectivity of the remaining snow cover as the temperature rises. For example, the grain size of the snow increases. Furthermore, there is the formation of liquid water on the ice, called pounding, as well as the expansion of bare ice areas (Tedesco et al., 2016a, 2011). From 1996 to 2012, the summer season albedo trend of the GIS was -4 % per decade. Future albedo losses exclusively driven by a warming climate are predicted to be alarmingly high with -15 % in 2100 relative to 2000 (Tedesco et al., 2016a). The decline in albedo is so alarming because it impacts the future strength of the SAF and thus results in a reinforcing circle and amplified loss of snow and

ice (Le clec'h et al., 2019).

Besides the concerning increase in global sea level rise, there is the possible threat that the GIS melts irreversibly after passing a potential tipping point (Robinson et al., 2012; Ridley et al., 2009). The GIS is currently the largest contributor to sea level rise, contributing even more than the Antarctic ice sheet (IPCC, 2019). This fact reveals why the GIS is a highly relevant element for potential tipping. Also, the reinforcing cycle of the SAF increases the hazard of tipping because the future increase in temperature accelerates. This, in turn, promotes the melting of the ice sheet and increases the likelihood that the GIS passes a tipping threshold. Although tipping points are uncertain, a rise in global atmospheric temperature of 1.5 to 2 °C to pre-industrial levels is a serious threat to the stability of the GIS (IPCC, 2018). More conservative calculations estimate the lower bound of a serious risk of tipping as low as 1°C (Calel and Stainforth, 2016). In general, two processes can cause tipping. First, as the ice melts at the surface, the GIS becomes thinner and is exposed to higher surface temperatures at lower elevations. This process is called *surface mass balance elevation feedback effect* (SMBE feedback). The second process is the SAF, which causes a higher absorption of solar radiation due to the melting of snow- and ice-covered surfaces. As a consequence, the surface heats up and accelerates the melting of the GIS (Pattyn et al., 2018).

This is the first work to integrate SAF into an Integrated Assessment Model (IAM). The extended model is named DICE-GIS SAF and is based on DICE-GIS (Nordhaus, 2019). I implement the SAF by modifying the climate feedback parameter. When modeling the SAF, I account for the loss of the albedo in three ways: (1) the albedo contrast between snow and ice, (2) the albedo of the remaining snow cover which changes its reflectivity due to metamorphysical processes within the snow cover, and (3) the actual loss of snow- and ice-covered areas, which causes a strong decrease in the reflectivity of the surfaces. Besides, I consider the SMBE feedback by modeling the melting behavior of the GIS volume to its surface area. Moreover, I integrate a tipping process that models the reinforcing cycle between the volume loss of the GIS and the temperature increase.

The economy of the DICE-GIS model (Nordhaus, 2019) is based on a neoclassical Ramsey growth model. Investment is not only dedicated to classical capital but also natural capital by devoting output to emission reduction. This leads to a decline in consumption today but increases consumption possibilities in the future. The major source of output growth per capita, in the long run, is an exogenous improvement in productivity. The social cost of carbon (SCC) is based on a cost-benefit analysis related to climate change mitigation and states the associated cost for each tonne of carbon dioxide emitted. Therefore, the SCC captures the cost of all future climate damages and determines the optimal policy by setting a Pigouvian tax equal to the SCC.

Taking the SAF into account is essential for determining the optimal policy, while additional tipping has only a minor impact on the SCC. Accounting for the SAF raises the SCC under the optimal policy from 274.92 to 319.67 $/t CO_2 in 2100, an increase of

16.3 %. The SCC shows a significantly higher peak value with 4,227.23 compared to 3,562.49 \$/t CO_2. The increase in SCC is mainly due to the accelerated rise in global temperature and less to the increased melting of the ice sheet. The SAF reduces the volume of the GIS in 3500 by 1.6 %, and raises the peak increase in global temperature from 4.13 to 4.31°C, an increase of 4 %. Additional accounting for tipping raises the SCC in 2100 up to 321.25 \$/t CO_2, a further increase of 0.5 %. The peak SCC raises up to 4,324.80 \$/t CO_2. Tipping reduces the volume further by up to 35.2 %. The amplified rise in temperature is the main channel through which the SAF affects the SCC. The accelerated volume loss of the GIS due to the SAF and potential tipping has a minor impact on the SCC.

There is a broad literature on the inclusion of earth system changes, tipping elements, and climate risks into IAMs (Kopp et al., 2016; Lenton and Schellnhuber, 2007; Lenton and Ciscar, 2012; Cai et al., 2015). Several papers describe concrete model extensions regarding the climate or carbon-cycle module. For instance, Dietz and Venmans (2019) integrate the saturation of carbon sinks into an analytical IAM. Lemoine and Traeger (2016) analyze climate policy with a potential domino effect of three different tipping points. Others expand the scope of IAMs by adding uncertainty which can be related to the hazard rate of tipping (Cai and Lontzek, 2019; Diaz and Keller, 2016), or the location of the tipping point (Naevdal, 2006; Lemoine and Traeger, 2014).

Moreover, there are several extensions specific to the DICE model (Nordhaus, 2017). Cai and Lontzek (2019) add climate and economic risk and model a collapse in ocean circulation. Moreover, Cai et al. (2016a) implement global spatial heat transport. Diaz and Keller (2016) include the potential tipping of the West Antarctic ice sheet. Heutel et al. (2016) incorporate solar geo-engineering and deal with different kinds of climate tipping points. Cai et al. (2016b) model the causal interaction between five potential tipping elements in the setting of a stochastic DICE version. Nordhaus (2019) includes the potential disintegration, i.e., the irreversible melting, of the GIS.

The tipping point in DICE-GIS SAF is reached endogenously, as in Lemoine and Traeger (2014); Diaz and Keller (2016). Other papers model it exogenously, as for instance in van der Ploeg (2014). I refrain from modeling stochastic tipping to benchmark DICE-GIS. Hence, I abstract from uncertainty and implement a deterministic tipping process and tipping threshold. This is in contrast to Cai and Lontzek (2019); Diaz and Keller (2016); Naevdal (2006); Lemoine and Traeger (2014) who model a stochastic tipping process. Furthermore, I model the consequence of tipping as a shift in the melting dynamic of the GIS, which simultaneously induces an endogenous acceleration of the climate dynamic because the climate feedback parameter decreases. This approach is close to Lemoine and Traeger (2014) who model the consequence as an irreversible change in climate sensitivity. However, the shift in the climate feedback parameter in their work is exogenous. Moreover, the consequences of tipping can be modeled through the affection of economic output, such as an abrupt and irreversible shock to total factor productivity

(de Zeeuw and van der Ploeg, 2014), a permanent shock to production (Cai and Lontzek, 2019), or through the impact on non-market goods (Cai et al., 2015). Besides, consequences can be expressed as a change in the capacity of the planet to absorb carbon (Lemoine and Traeger, 2014), or an abrupt and irreversible release of greenhouse gases from the ocean and the earth's surface (van der Ploeg, 2014).

The remainder of the paper is structured as follows: Section 2 provides the geophysical basics about albedo and the SAF. Section 3 sets up the implementation of DICE-GIS SAF and tipping. Section 4 describes the calibration. Section 5 presents the results and Section 6 concludes.

2 SAF Geophysics

Albedo and Climate Feedback Parameter

The albedo varies depending on the reflectivity of a given surface. In general, snow is very reflective and has a high albedo, whereas water, rock, and vegetation are more absorptive and have a lower albedo. The albedo reaches up to 0.9 for fresh snow. It reduces to 0.4 for melting snow. When dust and soot are deposited on the snow cover, the albedo declines to even 0.2 (Rees, 2019).

A climate feedback effect describes the reaction to an initial perturbation of the radiative system (Serreze and Barry, 2014). The reaction appears in the form of a change in temperature. Various climate feedbacks are affecting the global climate, such as the water vapor feedback or the SAF. Positive feedbacks accelerate the initial perturbation, while negative feedbacks dampen it. The SAF causes an additional amount of net shortwave radiation at the top of the atmosphere (TOA) and is, therefore, a positive feedback (Qu and Hall, 2007).

Overall, climate feedbacks are stronger in higher latitudes. So, the accelerating effect on temperature is higher in polar regions. This phenomenon is referred to as polar amplification (Goosse et al., 2018) and the SAF plays a crucial role for it (Hall, 2004). The albedo loss from the melting of ice and snow not only accelerates global warming but also starts a vicious circle because warmer temperatures in return accelerate the melting and in consequence promote the loss of albedo. As a result, polar temperatures rise by two to three times the global average (Serreze and Barry, 2011; Colman, 2013; Duan et al., 2019).

Regarding the melting of the GIS, the SAF is particularly important because of two facts. First, the cooling effect is diminishing because the average surface albedo declines with the enhanced melting of snow and ice. Second, the additional net solar radiation at the TOA is the most important factor for the massive melting during the summer season (Tedesco et al., 2016a).

Quantification

The albedo, $\alpha \in (0,1)$, is the ratio of the outgoing long-wave radiation, $S_{\uparrow}$, and the incoming short-wave radiation, $S_{\downarrow}$, i.e.,

$$\alpha = \frac{S_{\uparrow}}{S_{\downarrow}}. \tag{1}$$

Accordingly, the albedo gives the portion of the incoming short-wave radiation at the TOA, which is reflected by the earth's surface. Climate feedbacks are measured in the framework of climate feedback parameters which quantify the magnitude of a radiative perturbation for a given change in surface temperature. The feedback parameter for the SAF, denoted λ_{SAF}, is defined as the change in the radiative flux due to a change in surface temperature (Goosse et al., 2018). λ_{SAF} is given as, i.e.,

$$\lambda_{SAF} = \frac{\Delta F_{SAF}}{\Delta T_{SAF}} > 0, \tag{2}$$

where ΔF_{SAF} is the change in radiative forcing for a given change in temperature ΔT_{SAF}. Equation (2) illustrates the key assumption of the concept of climate feedback parameter stating that the change in radiative flux is proportional to the change in surface temperature. λ_{SAF} is positive because temperature increases with radiative forcing.

In more detail, the SAF is modeled by the change in the amount of net shortwave radiation at the TOA, Q_{net}, with the change in surface temperature, T_s (Qu and Hall, 2007). So the SAF, denoted $\frac{\partial Q_{net}}{\partial T_s}$, is given by

$$\frac{\partial Q_{net}}{\partial T_s} = -\, S_{\downarrow}\, \frac{\partial \alpha_p}{\partial \alpha_s}\, \frac{\Delta \alpha_s}{\Delta T_s}. \tag{3}$$

$S_{\downarrow}$ is assumed to be constant. So, $\frac{\partial Q_{net}}{\partial T_s}$ depends on the product of two terms: the first is the effect of the surface albedo, α_s, on the planetary albedo, α_p, and the second is the sensitivity of the surface albedo to temperature changes, $\frac{\Delta \alpha_s}{\Delta T_s}$. This sensitivity describes the change in α_s for each 1°C increase in surface temperature and is commonly used to approximate the SAF strength in climate models (Qu and Hall, 2014). Since polar warming affects the strength of the SAF due to albedo loss, $\frac{\Delta \alpha_s}{\Delta T_s}$ is of particular importance.

The magnitude of $\frac{\Delta \alpha_s}{\Delta T_s}$, in the following denoted NET effect, can be split into the SNC (snow cover) and the TEM (temperature) component (Thackeray and Fletcher, 2016). The NET effect is given as

$$\underbrace{\frac{\Delta \alpha_s}{\Delta T_s}}_{\text{NET}} = \underbrace{(\alpha_{snow} - \alpha_{ice})\, \frac{\Delta S_{snow}}{\Delta T_s}}_{\text{SNC}} + \underbrace{\bar{S}_{snow}\, \frac{\Delta \bar{\alpha}_{snow}}{\Delta T_s}}_{\text{TEM}}. \tag{4}$$

The SNC component in Equation (4) is related to exposed ice. It describes the re-

vealing of less reflective surfaces, mainly snow-free bare ice areas that appear after the snow cover on top of the ice has melted. These exposed surfaces have a lower albedo than snow-covered surfaces, leading to greater absorption of solar radiation. The SNC component is given by the contrast between the seasonal mean albedo of snow-covered surfaces, α_{snow}, and the albedo of ice but snow-free surfaces, α_{ice}. The difference in albedo is multiplied by the change of the snow cover extent, ΔS_{snow}, with respect to a change in surface temperature, ΔT_s. Whereby $\frac{\Delta S_{snow}}{\Delta T_s}$ states the fraction of the snow cover which melts for each 1°C increase in surface temperature.

The TEM component in Equation (4) is related to the metamorphysical characteristics within the snow cover. As the temperature increases, there are various changes within the snowpack. For example, the increase in snow grain size or the rise in water amount, which both influence the reflective properties of the snow cover (Helsen et al., 2017; Tedesco et al., 2016a). Thus, the albedo of snow changes with warming temperature even though no snow or ice is actually melting. The average snow-covered fraction, $\bar{S}_{snow}$, is multiplied by the sensitivity of the mean snow albedo to temperature increase, $\frac{\Delta \bar{\alpha}_{snow}}{\Delta T_s}$, with $\Delta \bar{\alpha}_{snow}$ denoting the change in mean snow albedo.

Since both components cause a reduction of the reflective properties of the surface, the NET effect describes the darkening of the ice sheet. The observed darkening of the GIS is strongly driven by the reduction of the snow cover extent (Tedesco et al., 2016a). Moreover, in 14 out of 17 climate models, the SNC component dominates the strength of the surface albedo sensitivity (Fletcher et al., 2015; Qu and Hall, 2007).

In conclusion, the NET effect, or $\frac{\Delta \alpha_s}{\Delta T_s}$, is the average sensitivity of snow-covered and snow-free areas in relation to a change in temperature and thus is used to approximate the strength of the SAF. Since the albedo declines with rising temperature, $\frac{\Delta \alpha_s}{\Delta T_s} < 0$.

$\frac{\Delta \alpha_s}{\Delta T_s}$ is multiplied by λ_{SAF} to model the corresponding change in the SAF feedback parameter due to the loss of albedo, denoted $\lambda_{\Delta SAF}$.

$$\lambda_{\Delta SAF} = \lambda_{SAF} \frac{\Delta \alpha_s}{\Delta T_s} T_s, \tag{5}$$

where T_s is the absolute rise in surface temperature, and it is $T_s > 0$. Since $\lambda_{SAF} > 0$, $\frac{\Delta \alpha_s}{\Delta T_s} < 0$ and $T_s > 0$, it follows $\lambda_{\Delta SAF} < 0$. So, the change in the strength of the SAF is modeled as a decline in the climate feedback parameter.

3 Numerical Implementation

Climate Feedback Parameter

To implement the SAF into DICE-GIS (Nordhaus, 2019), I integrate the effect of a specific albedo feedback into the climate module by modifying the already existing climate feedback parameter. The standard feedback parameter in DICE-GIS, denoted λ_{DICE}, is a globally aggregated parameter that captures all relevant feedback effects, for example,

cloud feedbacks but also the SAF (Calel and Stainforth, 2016). λ_{DICE} is constant over time and given as

$$\lambda_{DICE} = \frac{F_{CO_2}}{T_{CO_2}}. \tag{6}$$

F_{CO_2} refers to the radiative forcing from doubling the amount of carbon dioxide in the atmosphere and T_{CO_2} to the related rise in global temperature. T_{CO_2} is the climate sensitivity and is inferred from climate models that hold land ice sheets constant (Lemoine and Traeger, 2014). Hence, the current state of the GIS and the actual atmospheric temperature have no impact on λ_{DICE}.

General Modifications

Global warming has a stronger impact in the arctic regions because of arctic amplification (Serreze and Barry, 2011; Colman, 2013; Duan et al., 2019). To model the higher temperature increase on the GIS, I assume the arctic temperature, denoted T_{arc}, to rise twice as fast as the global atmospheric temperature, denoted T_{globe}. Therefore, I obtain

$$T_{arc}(t) = 2\ T_{globe}(t). \tag{7}$$

The damage function of DICE-GIS only considers the increase of the global atmospheric temperature. DICE-GIS SAF refers to the same damage function. Hence, T_{arc} has no direct influence on economic damages, but only affects them through the accelerated temperature increase due to the SAF. The higher T_{arc}, the more ice melts. The higher the albedo loss, the higher is the corresponding future rise in T_{globe} and in sea level, which directly impacts economic damages.

The implementation of the SAF requires the surface area of the GIS because the albedo refers to the spatial extent of the ice sheet. But, DICE-GIS includes only the volume of the GIS, denoted V, and does not take the surface area or height into account. Therefore, I include a relation of the GIS volume to its surface into DICE-GIS SAF.

To calculate the initial surface area of the GIS, denoted A_0, I divide the initial volume, denoted V_0, by the initial average height, denoted H_0, i.e., $A_0 = \frac{V_0}{H_0}$. To take the SMBE feedback into account, I assume that until a given threshold of V, denoted δ_V, the surface, denoted A, keeps its initial extent A_0, and the volume loss is only reflected by the thinning of the ice sheet, which I model through a proportional decline in H. After passing δ_V, A is shrinking according to a function of V and V_0. A is given as

$$A(t) = \begin{cases} A_0 & \text{for } V(t) \geq \ \delta_V \\ A_0 \ \dfrac{V(t)}{\eta\ V(t) + (1-\eta)\ \frac{\delta_V}{100}\ V_0} & \text{for } V(t) < \ \delta_V. \end{cases} \tag{8}$$

The underlying law and the derivation of Equation (8) can be found in Appendix A.

Moreover, the surface area fraction, denoted S, is given as $S(t) = \frac{A(t)}{A_0}$. The initial surface fraction is $S_0 = 1$. Furthermore, I split S into surface area covered with snow, S_{snow}, and surface area where the snow cover has melted and only ice remains behind, S_{ice}. Hence, $S(t) = S_{snow}(t) + S_{ice}(t)$. Remember that, the separation of snow- and ice-covered surface is important to model the strength of the SAF, i.e., the contrast in the reflective properties between snow and ice (SNC component), and the change in reflectivity on the remaining snow-covered surface area (TEM component). I assume that for the initial increase in global temperature, $T_{globe}(0) = 0.85$, the whole GIS is still covered with snow, thus $S_{snow}(0) = 1$ and $S_{ice}(0) = 0$.

Before passing δ_V, the increase in T_{arc} and the melting lead to a fall in S_{snow}, but in return rise S_{ice} by the same amount. After passing δ_V, it is $S(t) < 1$, and there is not only a decline of snow-covered areas but the surface area of the ice sheet is actually shrinking. The fraction of this former ice-covered surface where now less reflective bedrock appears, denoted L, is given as $L(t) = 1 - S(t)$.

SAF Implementation

In the following implementation, I abstract from a specific arctic surface temperature and use instead the arctic temperature which refers to the general atmospheric temperature in the Arctic region. Therefore, $T_s \equiv T_{arc}$.

Since the existing feedback parameter λ_{DICE} is a globally aggregated parameter, I only model the change of the SAF due to the melting of the GIS and then relate that change to λ_{DICE}. In more detail, I model the change of the SAF, denoted $\lambda_{\Delta SAF}$, by

$$\lambda_{\Delta SAF}(t) = \lambda_{SAF} \ \frac{\Delta \alpha_s}{\Delta T_{arc}}(t) \ T_{arc}(t). \tag{9}$$

λ_{SAF} captures the absolute contribution of the SAF to the global climate feedback parameter λ_{DICE}. $\frac{\Delta \alpha_s}{\Delta T_{arc}}$ is the sensitivity of the surface albedo to temperature, which I model endogenously according to the NET effect of Equation (4). Thereby, I model ΔS from the SNC component of Equation (4) by

$$\Delta S(t) = \frac{\gamma}{A(t)} = S_{melt}(t). \tag{10}$$

γ denotes the extent of the surface above which the snow cover melts when T_{arc} increases by 1°C. So, S_{melt} states the fraction of the surface area which melts for each 1°C increase in T_{arc}. Even tough γ is constant, S_{melt} increases over time as soon as δ_V is passed, and A, therefore, declines over time.

Moreover, I model $\bar{S}_{snow}$ from the TEM component of Equation (4) through two steps. First, I calculate the total surface fraction with melted snow cover, S_{ice}, for a given increase

in T_{arc} by

$$S_{ice}(t) = S_{melt}(t)\ T_{arc}(t). \tag{11}$$

Second, I subtract S_{ice} from 1 to get the fraction of surface which is still covered by snow, S_{snow}. Therefore, $\bar{S}_{snow} = 1 - S_{ice}(t) = S_{snow}(t)$. Through this approach, I endogenously determine the relative strength of the two components of the NET effect. Plugging S_{melt} and S_{snow} into Equation (4), and substituting T_s with T_{arc} yields

$$\underbrace{\frac{\Delta\alpha_s}{\Delta T_{arc}}(t)}_{\text{NET}} = [\underbrace{(\alpha_{snow} - \alpha_{ice})\ S_{melt}(t)}_{\text{SNC}} + \underbrace{S_{snow}(t)\ \frac{\Delta\alpha_{snow}}{\Delta T_{arc}}}_{\text{TEM}}]\ S(t). \tag{12}$$

To scale the effect to the remaining total surface area of the GIS, I multiply both components by the surface fraction S. This becomes important as δ_V is passed and $S(t) < 1$. Now, I calculate $\lambda_{\Delta SAF}$ from Equation (9) using Equations (7), (12), and λ_{SAF}.

In addition to the albedo loss from the darkening of the ice sheet, there is a further albedo loss as soon as δ_V is passed, and in consequence $S(t) < 1$ and $L(t) > 0$. Bedrock appears underneath the former ice-covered surface which has a significantly lower surface albedo than snow or ice. I assume that the entire reflective properties of the ice sheet surface are lost as soon as bedrock appears. As a result, the SAF disappears on this fraction of the surface. I scale the total loss of albedo, denoted λ_{Loss}, to the fraction of bedrock surface L. Therefore, I model the total albedo loss by

$$\lambda_{Loss}(t) = (-1)\ \lambda_{SAF}\ L(t). \tag{13}$$

In general, different climate feedback effects are approximately additive. So, different feedback parameters can be added together (Goosse et al., 2018; Duan et al., 2019; Colman, 2003). Hence, the overall time-dependent climate feedback parameter accounting for the albedo loss from the melting of the GIS, denoted λ_{FB}, is given by the sum of the original climate feedback parameter, λ_{DICE}, and the two feedback parameters related to the SAF. Therefore, I model λ_{FB} by

$$\lambda_{FB}(t) = \lambda_{DICE}\ +\ \underbrace{\lambda_{\Delta SAF}(t)\ +\ \lambda_{Loss}(t)}_{\text{Change in SAF from GIS melting}}\ . \tag{14}$$

So, λ_{FB} is the global climate feedback parameter accounting for the change of the SAF due to the melting of the GIS. Since the SAF is a positive feedback effect, the loss of albedo corresponds to a decline in the climate feedback parameter (Goosse et al., 2018; Duan et al., 2019). Therefore, it holds $\lambda_{\Delta SAF}(t) < 0$ and $\lambda_{Loss}(t) \leq 0$. In conclusion, $\lambda_{FB} < \lambda_{DICE}$. In contrast to λ_{DICE}, λ_{FB} is not constant but rather depends on $\frac{\Delta\alpha_s}{\Delta T_{arc}}$ and T_{arc}, or T_{globe}. This becomes apparent from Equation (7) and (9). Thus by taking the SAF into account, the feedback parameter depends on the current state of the GIS and more

specifically on the volume, or the surface area, and the global atmospheric temperature.

Since the SAF is a relatively responsive feedback effect (Hall, 2004), I model it without time delay. Therefore, $\frac{\Delta\alpha_s}{\Delta T_{arc}}$, or the NET effect, impacts the feedback parameter $\lambda_{\Delta SAF}$ and therefore λ_{FB} immediately, i.e., in the same time period as the fraction of melted snow S_{melt} from the SNC component or the average fraction of the snow-covered area S_{snow} from the TEM component changes. Besides, I abstract from any seasonal fluctuations of parameters or variables. Moreover, I do not consider the albedo loss due to contaminants on the surface of the ice sheet such as aerosol deposits, as there is no evidence that the accelerated darkening of the GIS is due to dust accumulation (Tedesco et al., 2016a).

SAF Integration

I integrate λ_{FB} into DICE-GIS SAF by replacing λ_{DICE} in the temperature equation of DICE-GIS. This gives

$$T_{globe}(t+1) = T_{globe}(t) + c_1[F_{CO2}(t+1) - \lambda_{FB}(t)\ T_{globe}(t)] - c_2[T_{globe}(t) - T_{oce}(t)],$$

with $F_{CO2}(t+1)$ denoting radiative forcing, $T_{oce}(t)$ denoting ocean temperature, c_1 denoting the transfer coefficient for the upper atmosphere, and c_2 denoting the transfer coefficient for the atmosphere to the ocean. It is $c_1, c_2 > 0$. The transfer coefficients can be interpreted as the speed with which the temperature converges to its new equilibrium. Both coefficients are directly taken from Nordhaus (2019).

Since $c_1 > 0$ and $\lambda_{FB}(t) < \lambda_{DICE}$, $T_{globe}(t+1)$ under λ_{FB} is always higher than under λ_{DICE}. This fact models the accelerating temperature increase due to the loss of albedo.

GIS Tipping

In contrast to Lemoine and Traeger (2014), the tipping in DICE-GIS SAF does not refer to an exogenous shift in the climate feedback parameter. Rather, it refers to a reinforced dynamic in the endogenous decline of the climate feedback parameter, which is induced by the accelerated melting of the GIS.

I model the tipping points as exogenous thresholds, denoted κ_V for the volume tipping threshold, or κ_T for the temperature tipping threshold. The tipping point κ_T reflects a global threshold and refers to T_{globe}. Both thresholds are reached endogenously within the model. Upon passing κ_V or κ_T, the melt rate of the GIS accelerates. Note that, the decrease of the volume in DICE-GIS is modeled as an absolute change of the volume. For the sake of simplicity, I call it melt rate when referring to the absolute change of the volume. I model the consequences of passing a tipping point by a tipping factor $\psi > 0$, which increases the melt rate of V. Furthermore, multiple tipping takes into account the successive passing of both thresholds, i.e., a combination of temperature and volume tipping. As soon as κ_V and κ_T are exceeded, I assume that the melt dynamic is further accelerated by the interaction between temperature increase, albedo loss, and melting of

the GIS. The rising temperature increases the loss of ice and in return, this increases the temperature through the SAF. Therefore, I exponentiate ψ with $\rho > 1$, for more information about the parameter value see Section 4 Calibration - Tipping.

The melt equation accounting for tipping, $\dot{V}_{TP}$, is given as

$$\dot{V}_{TP}(t) = \begin{cases} g(t) & \text{for } T_{globe}(t) < \kappa_T \text{ or } V(t) \geq \kappa_V \\ \psi \; g(t) & \text{for } T_{globe}(t) \geq \kappa_T \text{ or } V(t) < \kappa_V \\ \psi^\rho \; g(t) & \text{for } T_{globe}(t) \geq \kappa_T \text{ and } V(t) < \kappa_V. \end{cases} \tag{15}$$

where $g(t)$ is the standard melt function from DICE-GIS.

4 Calibration

The parameter choice of the model parameter is described in the following. Tables with the values of all parameters can be found in Appendix B.

Volume and Surface

The actual volume of the GIS is about 2,850,000 km^3 with an average thickness of 1.6 km (Nordhaus, 2019). This gives an actual surface area of 1,781,250 km^2. The initial volume is scaled such that $V_0 = 100$. Moreover, the initial height is $H_0 = 1.6$. The actual initial surface area A_0 is given the actual surface area divided by the scaling factor of 28,500, i.e., $A_0 = \frac{1{,}781{,}250}{28{,}500} = 62.5$. I assume the threshold δ_V to be 80 % of the initial volume, hence $\delta_V = 0.8\, V_0 = 80$. Regarding η it holds that the larger η, the more convex is the relation between A and V, see also Equation (8). I set $\eta = 0.45$ to define a slight convexity between the surface and the volume.

SAF

The literature states different estimates for the absolute contribution of the SAF to the climate feedback parameter λ_{SAF}. Flanner et al. (2011) estimate λ_{SAF} within the range of 0.33 to 1.07 with the best estimate of 0.62. Duan et al. (2019) calculate the average contribution of sea ice and land snow to the climate feedback parameter to be 0.77 with the separated effect for land snow of 0.3. Qu and Hall (2014) find a mean of 0.42 for the northern hemisphere while investigating 25 climate models. Winton (2006) provides an estimate for the mean λ_{SAF} of 0.3. Regarding these estimates, I choose the value of 0.5 for λ_{SAF}.

The value of α_{snow} reflects the albedo of the accumulation area.[1] It is estimated to be in the range of 0.75 to 0.83 (Alexander et al., 2014). Box et al. (2012) find a mean annual

[1] Area with positive mass balance, i.e., snow accumulation exceeds the melting of snow and ice discharge.

albedo for the accumulation area of 0.81. Moreover, observations from Greenland indicate snow albedo values within the range of 0.75 to 0.85 (Helsen et al., 2017; Alexander et al., 2014). Therefore, I set α_{snow} to 0.81.

The value of α_{ice} refers to the albedo of the ablation area.[2] Observations and estimation indicate that the value is in the range of 0.45 to 0.67 (Alexander et al., 2014; van Angelen et al., 2012; Box et al., 2012). Therefore, I set α_{ice} to 0.45.

According to the estimate of Abdalati and Steffen (1997), an increase in temperature of 1 °C over the GIS causes surface melting, and hence, a decline in the snow cover extent of $80,000\ km^2$. Hence, I choose the value of -80,000 for γ.

The value of $\frac{\Delta\alpha_{snow}}{\Delta T_{arc}}$ describes the sensitivity of the snow albedo to temperature changes. For the northern hemisphere, it is estimated to be within the range of -0.9 to -1.7 with a mean strength of -1.2 (Fletcher et al., 2015; Thackeray and Fletcher, 2016). Moreover, Box et al. (2012) find a mean sensitivity for the GIS accumulation area of -0.2, with extreme sensitivities up to -15.0 in the South-Western part of the ice sheet. According to these estimates, I set $\frac{\Delta\alpha_{snow}}{\Delta T_{arc}}$ equal to -1.2.

Tipping Thresholds

For volume tipping, I assume that as soon as there is only 90 % of the initial volume left, the disintegration of the GIS is difficult to reverse. Hence, $\kappa_V = 0.9\, V_0 = 90$. This specification is based on the estimates of Ridley et al. (2009). The threshold is reasonable as the GIS has thinned considerably until $V < \kappa_V$. Due to the lower elevation of the ice sheet, the ice is exposed to higher surface temperatures which accelerates the melting process.

Temperature tipping is based on the passing of a certain temperature threshold, κ_T. Irreversible melting of the GIS is likely for a global temperature increase in the range of 0.8 to 3.2°C (Robinson et al., 2012), or 1.3 to 4.5°C (Ridley et al., 2009). These results agree with the IPCC's assessment that assumes a serious risk of tipping from a temperature increase of 1.5 to 2°C (IPCC, 2019). I set $\kappa_T = 3.4$°C.

Furthermore, I assume that after passing a potential tipping point the melt rate doubles its intensity, hence $\psi = 2$. Moreover, for multiple tipping, I assume that as soon as both tipping points are reached, the intensified melt rate is exponentiated by $\rho = 2$ to model the increasing instability of the GIS.

I run the model with a five-year time step from 2015 to 3500. Besides the noted changes, I change the value of one additional parameter. For period $t = 2015$ to 2115, I set the upper limit of the emission control rate from 1.2 to 1.0 to restrict the impact of geo-engineering and prevent jumping of emission control due to the default calibration in Nordhaus (2019). Apart from this, the model setting of DICE-GIS SAF remains the same as in DICE-GIS.

[2] Area with negative mass balance, i.e., the melting of snow and ice discharge exceed the snow accumulation.

5 Results

The following results describe the optimal policy, i.e., the policy under which external climate damages are fully internalized. Hence, the carbon price equals the SCC. DICE-GIS refers to the model of Nordhaus (2019), while DICE-GIS SAF refers to my extended model with the integrated SAF module. Results for the non-optimal policy, under which climate damages are not internalized, are presented in Appendix C.

SCC under Optimal Policy

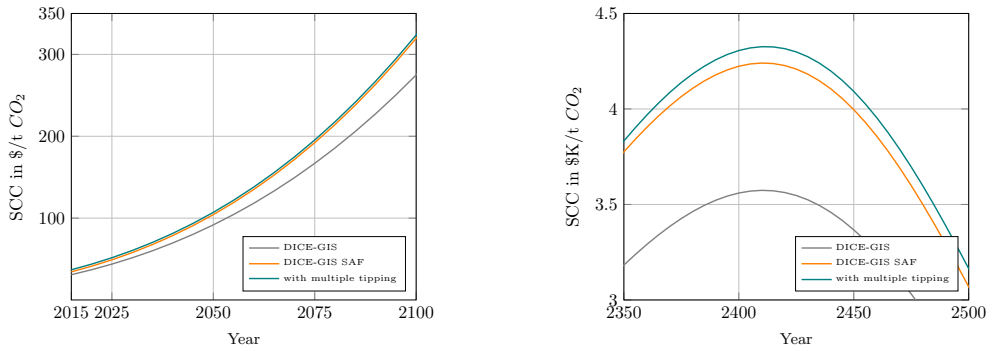

(a) SCC until 2100

(b) peak SCC

Figure 1: SCC

Figure 1(a) shows the SCC until 2100 and Figure 1(b) presents the peak values for the SCC from 2350 to 2500. The gray graph refers to DICE-GIS, the orange graph to DICE-GIS SAF, and the green graph to DICE-GIS SAF with multiple tipping. Accounting for the SAF raises the SCC from 274.92 to 319.67 \$/tCO_2 in 2100, an increase of 16.3 %. In contrast to the SAF, the additional hazard of multiple tipping has only a minor impact on the SSC. The SCC in 2100 increase to 321.25 \$/tCO_2, an additional increase of only 0.5 %. Besides, the SAF raises the peak value of the SCC. For DICE-GIS, the SCC peaks at 3,573.91 \$/tCO_2, while for DICE-GIS SAF at 4,240.50 \$/tCO_2, an increase of 18.6 %. The peak value for DICE-GIS SAF with multiple tipping is 4,326.03 \$/tCO_2; a further increase of 2 %. Figure 1 depicts that the SAF has a greater impact on the SCC than tipping.

GIS Dynamics

The following years are important for the understanding of the dynamics below: 2095, 2380, and 2560. 2095 is the year when the first tipping threshold κ_T is passed, therefore, the melting rate doubles for DICE-GIS with multiple tipping. In 2380, the second tipping threshold κ_V is reached as well, therefore, the melting rate accelerates further. In 2560, the volume threshold δ_V is exceeded and, in consequence, the surface area of the GIS starts to shrink.

Figure 2 presents the volume of the GIS on the left axis (solid lines) and the surface fraction of this GIS on the right axis (dashed lines) from 2015 to 3500. In 3500, the volume

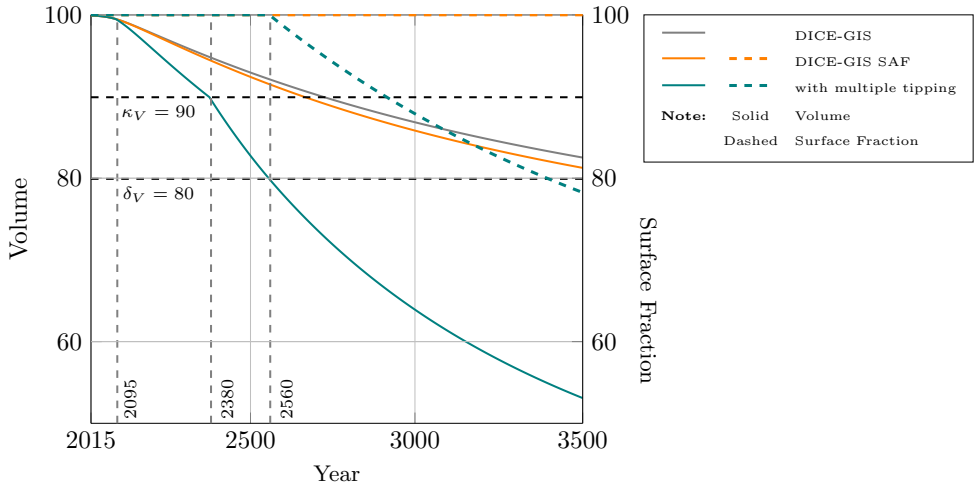

Figure 2: Volume and Surface Fraction

is 82.52 for DICE-GIS and 81.26 for DICE-GIS SAF. Comparing the solid gray and solid orange line, the calculations show that the SAF has per se only a small influence on the volume. Hence, neither of them reaches δ_V. Therefore, the surface keeps its initial size in both models. For DICE-GIS SAF with multiple tipping, the volume melts remarkably faster. Figure 2 shows that the first threshold κ_T is passed in 2095, see also Figure 4. The second threshold κ_V is reached in 2380. Moreover, DICE-GIS SAF passes δ_V in 2560 which is when the surface fraction starts to shrink. In comparison to DICE-GIS, the volume for DICE-GIS SAF with multiple tipping in 3500 is 53.08, or -35 %, while the surface fraction is 78 %. Figure 2 reveals that tipping has a greater impact on the volume of the GIS than the SAF.

The differences in the volume loss can be explained with the distinct melt dynamics displayed in Figure 3. The melt rate of DICE-GIS SAF is slightly more negative than of

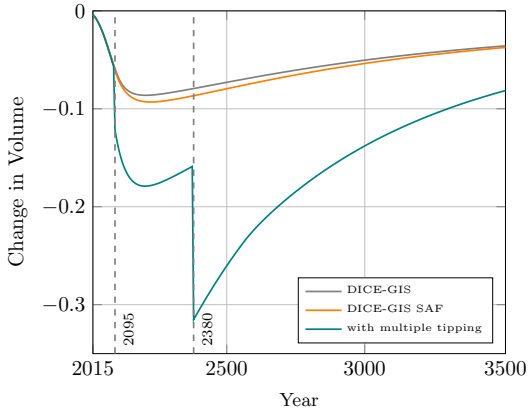

Figure 3: Melt Rate

DICE-GIS. This difference is due to the SAF. Regarding DICE-GIS SAF with multiple tipping, the melt rate is far more negative. As soon as κ_T is passed in 2095, the melt rate

is accelerated by the tipping factor ψ. As soon as κ_V is reached as well, i.e., in 2380, the melt rate is multiplied by the exponentiated factor ψ^ρ, i.e., by 4. Hence, the melt rate doubles again and falls from -0.16 to -0.32. However, this change in the volume of the GIS is induced more by the tipping dynamic than by the SAF. In conclusion, the SAF does not play a major role in the amplification of the melt dynamic, but tipping does. This is plausible, since tipping has a direct impact on the melt rate, and thus, on the volume. In contrast, the SAF influences the volume only indirectly through the decease in the feedback parameter which in turn increases the temperature and then accelerates the melting.

Temperature Dynamics

Figure 4 shows the temperature increase T_{globe} on the left axis (solid lines) and the feedback parameter on the right axis (dashed lines) from 2015 to 3500. Regarding the temperature

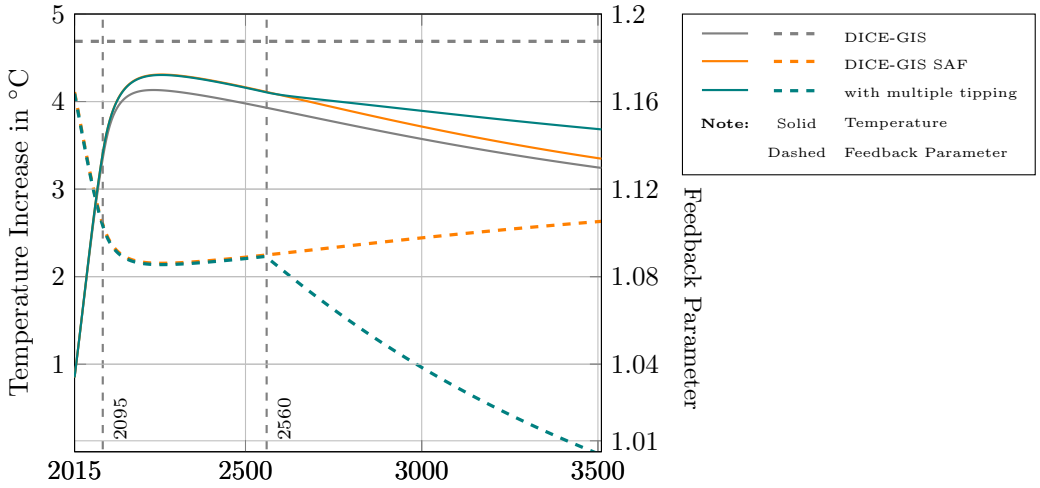

Figure 4: Temperature Increase and Feedback Parameter

increase, the threshold κ_T is passed in 2095. When accounting for the SAF, warming peaks in 2260 at 4.31°C, an additional increase in peak temperature of 4%. It is noticeable that warming peaks at the same time when the feedback parameter reaches its minimum value. The temperature rise of DICE-GIS SAF with multiple tipping does not flatten out as much, which is due to the stronger decreasing feedback parameter. In 3500, the temperature increase is 3.24°C for DICE-GIS, 3.35°C for DICE-GIS SAF, and 3.69°C for DICE-GIS SAF with multiple tipping.

The feedback parameter λ_{DICE} is 1.19 and constant over time. In contrast, the feedback parameter λ_{FB} decreases due to the SAF. Until 2260 λ_{FB} falls to 1.09. Then, the decrease is followed by stabilization. For DICE-GIS SAF the feedback parameter increases slightly after 2500. This means that the albedo loss decreases as the melting of the GIS slows down. Besides, less snow and ice melt on the surface as the temperature cools down again. For DICE-GIS SAF with multiple tipping, the feedback parameter decreases further from 2560, although the temperature starts to cool down. This is due

to the shrinking surface, see Figure 2, which causes a loss in total albedo. In 3500, λ_{FB} is 1.11 for DICE-GIS SAF and 0.99 for DICE-GIS SAF with multiple tipping. Accounting for the SAF decreases the feedback parameter by -7 %, or -17 % respectively.

Figure 4 depicts that the peak increase in temperature is caused by the SAF, while tipping has no significant influence on the temperature. Tipping only weakens the later cooling of the temperature, but the SAF intensifies the initially strong increase in temperature.

SAF and Tipping Implications

In summary, the presented results show interesting implications of the SAF and tipping, namely: the SAF increases the SCC because it amplifies the temperature increase due to the lower feedback parameter; while tipping enhances the volume loss of the GIS. As can be seen in Figure 4, the SAF has an earlier impact on the temperature increase than the tipping process. Hence, the damage from temperature increase induced by the SAF occurs earlier than the damage induced by tipping. Besides, additional damages from sea level rise caused by tipping occur only in the long term and therefore have less impact on the SCC. Consequently, damages from tipping lie in the far future. Even at very low discount rates, i.e., a higher valuation for future damages, accounting for multiple tipping does not significantly raise the SCC. This is true for the inclusion of multiple tipping in DICE-GIS and DICE-GIS SAF. Results for the corresponding SCC under varying discount rates are shown in Table 1. There is no significant difference in the SCC whether the calculation is done with or without multiple tipping. However, there is a significant difference once the SAF is accounted for. This confirms my conclusion that the SAF and not tipping is the main reason for the increase in the SCC. Thereby, the temperature increase is the most important channel through which the SAF affects the SCC.

Discounting	0.5 %	1 %	1.5 %[3]
DICE-GIS	757.42	418.15	274.92
with multiple tipping	757.45	420.71	276.29
DICE-GIS SAF	873.34	485.23	319.68
with multiple tipping	873.35	488.30	321.25

Table 1: SCC (\$/t CO_2) in 2100 depending on the discount rate

Robustness

In Appendix D, I show that the SCC and the volume of the GIS are robust (changes below 1 %) with regard to η (± 50 %) and δ_V (± 5 %). Moreover, the SCC is relatively robust (changes below 5 %) with regard to ρ (± 25 %) and γ (± 25 %). The SCC is sensitive (changes above 5 %) with regard to λ_{SAF} (± 50 %). Additionally, the feedback

[3]This is the standard DICE discount rate; it is used for the calculation of all results.

parameter is sensitive to λ_{SAF} ($\pm$ 50 %). However, this fact does not diminish my results but rather underlines that the SAF plays an important role for the temperature increase and therefore has a significant impact on SCC. Furthermore, the SCC and the volume are sensitive to ψ (-25 % to +100 %), especially to values of ψ greater than +50 %, because the tipping factor is exponentiated. Nevertheless, this parameter only influences multiple tipping and therefore does not diminish the importance of the SAF. A comprehensive sensitivity analysis can be found in Appendix D.

6 Conclusion

Although DICE-GIS (Nordhaus, 2019) takes the melting of the GIS into account for the estimation of the SCC, it does not consider any further feedback effects on the climate or sea level. As a result, the SCC is considerably underestimated. My extended DICE-GIS SAF model shows that it is not so much the sole melting of the GIS that raises the SCC, but rather the positive feedback effect arising from the loss of albedo. This, in turn, comes along with enhanced global warming and induces a vicious cycle between the melting of snow and ice, and temperature increase.

Accounting for the SAF raises the SCC in 2100 from 274.92 to 319.67 \$/t CO_2. The SCC shows a peak value of 4,227.23 compared to 3,562.49 \$/t CO_2. Additional tipping raises the peak SCC to 4,324.80 \$/t CO_2. The results for the year 2100 show that the increase in the SCC is mainly caused by the SAF with an increase of 16.3 %, and less by tipping, which causes an additional increase of only 0.5 %. This underlines that the inclusion of the SAF has a significant impact on the SCC. Furthermore, the SAF raises the peak temperature increase from 4.13 to 4.31°C. The temperature increase is the main channel through which the SAF impacts the SCC. The long-term volume of the GIS in 3500 declines by 1.6 %, while tipping reduces it further by up to 35.2 %. Tipping, therefore, plays a major role in the enhanced volume loss.

In conclusion, the consequent loss of albedo is a crucial factor in estimating future economic damage and determining the optimal policy. Given this insight, the optimal policy must not only be adopted but also enforced more consistently than it has been the case so far. The future carbon price must be based on the precise SCC to mitigate the melting of the GIS and preserve the cooling effect of the ice sheet on the global climate.

DICE-GIS SAF covers the role of the GIS only. The fact that the GIS is not the only large ice sheet on the planet emphasizes the great significance of the albedo loss on the SCC. All policy implications of my model can be transferred to the real world accounting for other ice sheets, sea ice, or even the entire cryosphere on the planet. Even if Antarctica is not yet melting as strongly as the GIS, with a total potential of about 59 m in global sea level rise as well as the possible loss of the largest and most reflective area of the planet (IPCC, 2014), it holds an enormous potential to increase the SCC even further. In addition, I focus exclusively on the contrast between snow-covered and bare

ice or bedrock-covered areas. However, when the melting of sea ice is also taken into account, the albedo loss is even higher because the contrast in reflectivity between sea ice and open ocean is more extreme. As a result, the climate heats up even more and the economic damage is even greater, leading to an even higher increase in the SCC.

Even though the time horizon, especially for the significant melting and tipping of the GIS is very long, there is already a noticeable increase in the SCC of 16.3 % by 2100. Besides, potential interactions with other earth components, which are likely to tip earlier, such as the irreversible thawing of the permafrost, could dramatically shorten the time horizon and move the tipping of the GIS much closer to the present. This would further exacerbate the albedo loss and strengthen the vicious cycle. For this reason, policymakers must already take the consequences of the melting of the GIS very seriously today, even if they seem far off at this stage.

The impact of the SAF on global warming is certain and already evident in the short term, but tipping is supposed to happen in the long run. Additionally, uncertainty from potential future interactions with other earth components plays a crucial role in long-term considerations. However, considering solely the tipping of the GIS without any interactions of other earth components, as in DICE-GIS SAF, uncertainty is rather not relevant. But the inclusion of uncertainty would be very important if long-term further interactions, such as the interaction with the North Atlantic Oscillation, are taken into account.

Without doubt, DICE-GIS SAF is based on various assumptions and simplifications. On the one hand, the assumed linear melting behavior which is taken from Nordhaus (2019) is not representative of the actual melting dynamic of the GIS (Trusel et al., 2018). On the other hand, the SAF is implemented in a simplified way, as well. The modeling does not account for seasonal variability or possible future changes in the cryospheric system, such as a change in the precipitation pattern. Nonetheless, DICE-GIS SAF provides a reasonable approach on how to simplify complex earth dynamics and integrate them into existing IAMs. To render the model more realistic, future work may include seasonable variability of the melting process, especially concerning the snow cover and the albedo. Moreover, future work may not only account for the volume loss of the GIS due to the melting but also due to the discharge of ice.

Above all, my research depicts that the SAF increases the SCC significantly due to the amplified temperature increase. This fact highlights the general importance of improving IAMs by integrating components of the earth system in a more detailed way than the popular state of the art IAMs do so far. Moreover, future research on the estimation of the SCC must include other potential feedback effects within different elements of the earth system and interactions across them. Otherwise, policymakers would be relying on what appears to be the optimal policy, taking an immense risk for future generations.

References

Abdalati, W. and Steffen, K. (1997). Snowmelt on the Greenland ice sheet as derived from passive microwave satellite data. *Journal of Climate*, 10(2):165–175.

Alexander, P., Tedesco, M., Fettweis, X., van de Wal, R., Smeets, C., and van den Broeke, M. (2014). Assessing spatio-temporal variability and trends in modelled and measured Greenland ice sheet albedo (2000-2013). *The Cryosphere*, 8(6):2293–2312.

Bamber, J., Griggs, J., Hurkmans, R., Dowdeswell, J., Gogineni, S., Howat, I., Mouginot, J., Paden, J., Palmer, S., Rignot, E., and Steinhage, D. (2013). A new bed elevation dataset for greenland. *The Cryosphere*, 7(2):499–510.

Box, J., Fettweis, X., Stroeve, J., Tedesco, M., Hall, D., and Steffen, K. (2012). Greenland ice sheet albedo feedback: Thermodynamics and atmospheric drivers. *The Cryosphere Discussions*, 6:821–839.

Cai, Y.and Judd, K., Lenton, T., Lontzek, T., and Narita, D. (2015). Environmental tipping points significantly affect the cost-benefit assessment of climate policies. *Proceedings of the National Academy of Sciences*, 112(15):4606–4611.

Cai, Y., Brock, W., and Xepapadeas, A. (2016a). Climate change economics and heat transport across the globe: Spatial DSICE. *Conference Paper Agricultural and Applied Economics Association*.

Cai, Y., Lenton, T., and Lontzek, T. (2016b). Risk of multiple interacting tipping points should encourage rapid CO2 emission reduction. *Nature Climate Change*, 6:520–525.

Cai, Y. and Lontzek, T. (2019). The social cost of carbon with economic and climate risks. *Journal of Political Economy*, 127(6):2684–2734.

Calel, R. and Stainforth, D. (2016). On the physics of three Integrated Assessment Models. *Bulletin of the American Meteorological Society*, 98:1199–1216.

Colman, R. (2003). A comparison of climate feedbacks in General Circulation Models. *Climate Dynamics*, 20:865–873.

Colman, R. (2013). Surface albedo feedbacks from climate variability and change. *Journal of Geophysical Research: Atmospheres*, 118(7):2827–2834.

de Zeeuw, A. and van der Ploeg, F. (2014). Climate tipping and economic growth: Precautionary saving and the social cost of carbon. Technical Report 9982, CEPR Discussion Papers.

Diaz, D. and Keller, K. (2016). A potential disintegration of the West Antarctic ice sheet: Implications for economic analyses of climate policy. *American Economic Review*, 106(5):607–11.

Dietz, S. and Venmans, F. (2019). Cumulative carbon emissions and economic policy: In search of general principles. *Journal of Environmental Economics and Management*, 96:108–129.

Duan, L., Cao, L., and Caldeira, K. (2019). Estimating contributions of sea ice and land snow to climate feedback. *Journal of Geophysical Research: Atmospheres*, 124(1):199–208.

Flanner, M., Shell, K., Barlage, M., Perovich, D., and Tschudi, M. (2011). Radiative forcing and albedo feedback from the Northern Hemisphere cryosphere between 1979 and 2008. *Nature Geoscience*, 4:151–155.

Fletcher, C., Thackeray, C., and Burgers, T. (2015). Evaluating biases in simulated snow albedo feedback in two generations of climate models. *Journal of Geophysical Research: Atmospheres*, 120(1):12–26.

Fürst, J., Goelzer, H., and Huybrechts, P. (2015). Ice-dynamic projections of the Greenland ice sheet in response to atmospheric and oceanic warming. *The Cryosphere*, 9(3):1039–1062.

Goosse, H., Kay, J., Armour, K., Bodas-Salcedo, A., Chepfer, H., Docquier, D., Jonko, A., Kushner, P., Lecomte, O., Massonnet, F., Park, H., Pithan, F., Svensson, G., and Vancoppenolle, M. (2018). Quantifying climate feedbacks in polar regions. *Nature Communications*, 9(1).

Hall, A. (2004). The role of surface albedo feedback in climate. *Journal of Climate*, 17:1550–1568.

Helsen, M., van de Wal, R., Reerink, T., Bintanja, R., Madsen, M., Yang, S., Li, Q., and Zhang, Q. (2017). On the importance of the albedo parameterization for the mass balance of the Greenland ice sheet in EC-Earth. *The Cryosphere*, 11(4):1949–1965.

Heutel, G., Moreno-Cruz, J., and Shayegh, S. (2016). Climate tipping points and solar geoengineering. *Journal of Economic Behavior & Organization*, 132:19–45.

IPCC (2014). Fifth Assessment Report (AR5) observed climate change impacts. Technical report, World Meteorological Organization, Geneva, Switzerland.

IPCC (2018). Global warming of 1.5°C. An IPCC Special Report on the impacts of global warming of 1.5°C above pre-industrial levels and related global greenhouse gas emission pathways, in the context of strengthening the global response to the threat of climate change, sustainable development, and efforts to eradicate poverty. Technical report, World Meteorological Organization, Geneva, Switzerland.

IPCC (2019). IPCC special report on the ocean and cryosphere in a changing climate. Technical report, World Meteorological Organization, Geneva, Switzerland.

Kopp, R., Shwom, R., Rachael, L., Wagner, G., and Yuan, J. (2016). Tipping elements and climate economic shocks: Pathways toward integrated assessment. *Earth's Future*, 4(8):346–372.

Le clec'h, S., Charbit, S., Quiquet, A., Fettweis, X., Dumas, C., Kageyama, M., Wyard, C., and Ritz, C. (2019). Assessment of the Greenland ice sheet - Atmosphere feedbacks for the next century with a regional atmospheric model coupled to an ice sheet model. *The Cryosphere*, 13(1):373–395.

Lemoine, D. and Traeger, C. (2014). Watch your step: Optimal policy in a tipping climate. *American Economic Journal: Economic Policy*, 6(1):137–166.

Lemoine, D. and Traeger, C. (2016). Economics of tipping the climate dominoes. *Nature Climate Change*, 6:514–520.

Lenton, T. and Ciscar, J. (2012). Integrating tipping points into climate impact assessments. *Climatic Change*, 117:585–597.

Lenton, T. and Schellnhuber, H. (2007). Tipping the scales. *Nature Climate Change*, 1:97–98.

Naevdal, E. (2006). Dynamic optimization in the presence of threshold effects when the location of the threshold is uncertain - with an application to a possible disintegration of the Western Antarctic Ice Sheet. *Journal of Economic Dynamics and Control*, 30(7):1131–1158.

Nghiem, S., Hall, D., Mote, T., Tedesco, M., Albert, M., Keegan, K., Shuman, C., DiGirolamo, N., and Neumann, G. (2012). The extreme melt across the Greenland ice sheet in 2012. *Geophysical Research Letters*, 39(20):L20502.

Nordhaus, W. (2017). Revisiting the social cost of carbon. *Proceedings of the National Academy of Sciences*, 114(7):1518–1523.

Nordhaus, W. (2019). Economics of the disintegration of the Greenland ice sheet. *Proceedings of the National Academy of Sciences*, 25(116):12261–12269.

Pattyn, F., Ritz, C., Hanna, E., Asay-Davis, X., DeConto, R., Durand, G., Favier, L., Fettweis, X., Goelzer, H., Golledge, N., Munneke, P., Lenaerts, J., Nowicki, S., Payne, A., Robinson, A., Seroussi, H., Trusel, L., and van den Broeke, M. (2018). The Greenland and Antarctic ice sheets under 1.5° C global warming. *Nature Climate Change*, 8:1053–1061.

Qu, X. and Hall, A. (2007). What controls the strength of snow-albedo feedback? *Journal of Climate*, 20:3971–3981.

Qu, X. and Hall, A. (2014). On the persistent spread in snow-albedo feedback. *Climate Dynamics*, 42:69–81.

Rees, W. (2019). *Remote Sensing of Snow and Ice*. Taylor & Francis Group.

Ridley, J., Gregory, J., Huybrechts, P., and Lowe, J. (2009). Thresholds for irreversible decline of the Greenland ice sheet. *Climate Dynamics*, 35:1049–1057.

Robinson, A., Calov, R., and Ganopolski, A. (2012). Multistability and critical thresholds of the Greenland ice sheet. *Nature Climate Change*, 2:429–429.

Serreze, M. and Barry, R. (2011). Processes and impacts of Arctic amplification: A research synthesis. *Global and Planetary Change*, 77:85–96.

Serreze, M. and Barry, R. (2014). *The Arctic Climate System*. Cambridge University Press, 2 edition.

Tedesco, M., Doherty, S., Fettweis, S., Alexander, P., Jeyaratnam, J., and Stroeve, J. (2016a). The darkening of the Greenland ice sheet: Trends, drivers, and projections (1981 - 2100). *The Cryosphere*, 10(2):477–496.

Tedesco, M. and Fettweis, X. (2019). Unprecedented atmospheric conditions (1948-2019) drive the 2019 exceptional melting season over the Greenland ice sheet. *The Cryosphere Discussions*, in review.

Tedesco, M., Fettweis, X., van den Broeke, M., van de Wal, R., Smeets, C., van de Berg, W., Serreze, M., and Box, J. (2011). The role of albedo and accumulation in the 2010 melting record in Greenland. *Environmental Research Letters*, 6(1):014005.

Tedesco, M., Mote, T., Fettweis, X., Hanna, E., Jeyaratnam, J., Booth, J., Datta, R., and Briggs, K. (2016b). Arctic cut-off high drives the poleward shift of a new Greenland melting record. *Nature Communications*, 7.

Thackeray, C., Derksen, C., Fletcher, C., and Hall, A. (2019). Snow and climate: Feedbacks, drivers, and indices of change. *Climate Change Reports*, 5:322–222.

Thackeray, C. and Fletcher, C. (2016). Snow albedo feedback: Current knowledge, importance, outstanding issues and future directions. *Progress in Physical Geography*, 40:392–408.

Trusel, L., Das, S., and Osman, M. (2018). Nonlinear rise in Greenland runoff in response to post-industrial Arctic warming. *Nature*, 564:104–108.

van Angelen, J., Lenaerts, J., Lhermitte, S., Fettweis, X., Kuipers Munneke, P., van den Broeke, M., van Meijgaard, E., and Smeets, C. (2012). Sensitivity of Greenland ice sheet surface mass balance to surface albedo parameterization: A study with a regional climate model. *The Cryosphere*, (5):1175–1186.

van der Ploeg, F. (2014). Abrupt positive feedback and the social cost of carbon. *European Economic Review*, 67:28–41.

Winton, M. (2006). Surface albedo feedback estimates for the AR4 climate models. *Journal of Climate*, 19:359–365.

A Derivation of Equation (8)

Equation:

$$A(t) = \begin{cases} A_0 & \text{for } V(t) \geq \delta_V \\ A_0 \, \dfrac{V(t)}{\eta \, V(t) + (1-\eta) \, \frac{\delta_V}{100} \, V_0} & \text{for } V(t) < \delta_V. \end{cases}$$

Assumptions:

1. $A(t) = \frac{V(t)}{H(t)}$
2. $\dot{H}(t) = \eta_1 \, \dot{V}(t)$ for all t with $V(t) \geq \delta_V$, whereby $\eta_1 = 1/A_0$
3. $\dot{H}(t) = \eta_2 \, \dot{V}(t)$ for all t with $V(t) < \delta_V$, whereby $\eta_2 = \eta/A_0$ and $\eta \in (0, 1)$

Case: $V(t) \geq \delta_V$
I assume that $A(t) = A_0$, i.e., the surface area is the initial surface area and is constant over time. According to Assumption 2, the growth rate of $H(t)$, denoted $\dot{H}(t)$, is given as

$$\dot{H}(t) = \frac{\dot{V}(t)}{A_0},$$

with $\dot{V}(t)$ denoting the growth rate of $V(t)$. Integrating $\dot{H}(t)$ gives

$$H(t) = \frac{V(t)}{A_0} + \sigma_1.$$

σ_1 is chosen such that

$$H_0 = \frac{V_0}{A_0}.$$

Hence, $\sigma_1 = 0$, and thus

$$H(t) = \frac{V(t)}{A_0}.$$

Under Assumption 1, it follows for $V(t) \geq \delta_V$

$$A(t) = \frac{V(t)}{H(t)} = \frac{V(t)}{\frac{1}{A_0} V(t)} = A_0.$$

Case: $V(t) < \delta_V$
According to Assumption 3, it is

$$\dot{H}(t) = \frac{\eta \, \dot{V}(t)}{A_0}.$$

Integrating $\dot{H}(t)$ gives

$$H(t) = \frac{\eta \, V(t)}{A_0} + \sigma_2.$$

σ_2 is chosen such that $H(t)$ is a continuous function with t^* denoting the period when δ_V is reached. Hence, $V(t^*) = \delta_V$. This gives

$$H(t^*) = \frac{V(t^*)}{A_0} = \frac{\delta_V}{100} \frac{V_0}{A_0}.$$

Therefore, it follows for σ_2

$$\sigma_2 = \frac{\delta_V}{100} \frac{V_0}{A_0} - \frac{\eta \frac{\delta_V}{100} V_0}{A_0} = \frac{(1-\eta)}{A_0} \frac{\delta_V}{100} V_0.$$

For $t \geq t^*$ it follows

$$H(t) = \frac{\eta V(t)}{A_0} + \frac{(1-\eta)}{A_0} \frac{\delta_V}{100} V_0.$$

Under Assumption 1, it follows for $V(t) < \delta_V$

$$A(t) = \frac{V(t)}{H(t)} = \frac{V(t)}{\frac{\eta}{A_0} V(t) + \frac{(1-\eta)}{A_0} \frac{\delta_V}{100} V_0} = A_0 \frac{V(t)}{\eta V(t) + (1-\eta) \frac{\delta_V}{100} V_0}.$$

B Calibration Tables

Parameter	V_0	H_0	A_0	δ_V	η
Value	100	1.6	62.5	80	0.45

Table A1: Parameters Volume and Surface

Parameter	λ_{SAF}	α_{snow}	α_{ice}	γ	$\frac{\Delta\alpha_{snow}}{\Delta T_{arc}}$
Value	0.5	0.81	0.45	-80,000	-1.2

Table A2: Parameters SAF

Parameter	κ_V	κ_T	ψ	ρ
Value	90	3.4	2	2

Table A3: Parameters Tipping

C Non-Optimal Policy Results

The results for the non-optimal policy are presented in the following. The main difference to the results for the optimal policy is mentioned.

SCC under Non-Optimal Policy

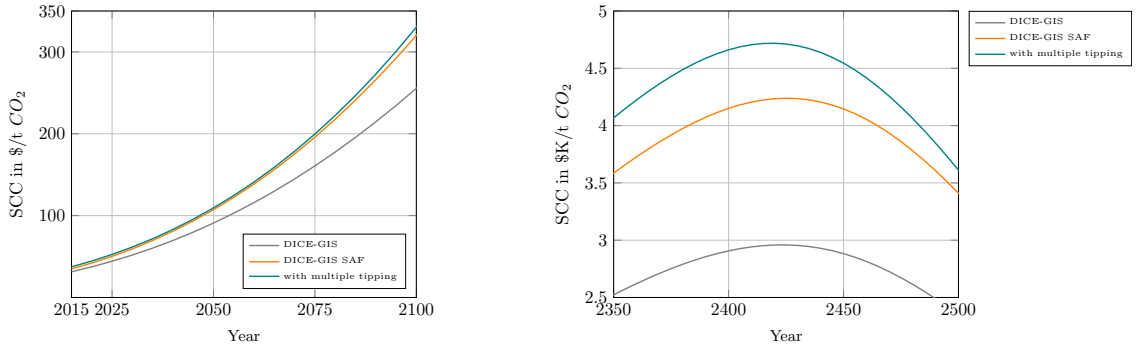

(a) SCC until 2100

(b) peak SCC

Figure A1: SCC

Figure A1(a) shows the SCC until 2100 and Figure A1(b) presents the peak values for the SCC from 2350 to 2500. The gray graph refers to DICE-GIS, the orange graph to DICE-GIS SAF, and the green graph to DICE-GIS SAF with multiple tipping.

The peak SCC for DICE-GIS is remarkably lower than under the optimal policy. When accounting for the SAF, the SCC is a little higher and the difference in the SCC between DICE-GIS SAF and DICE-GIS SAF with multiple tipping is larger.

GIS Dynamics

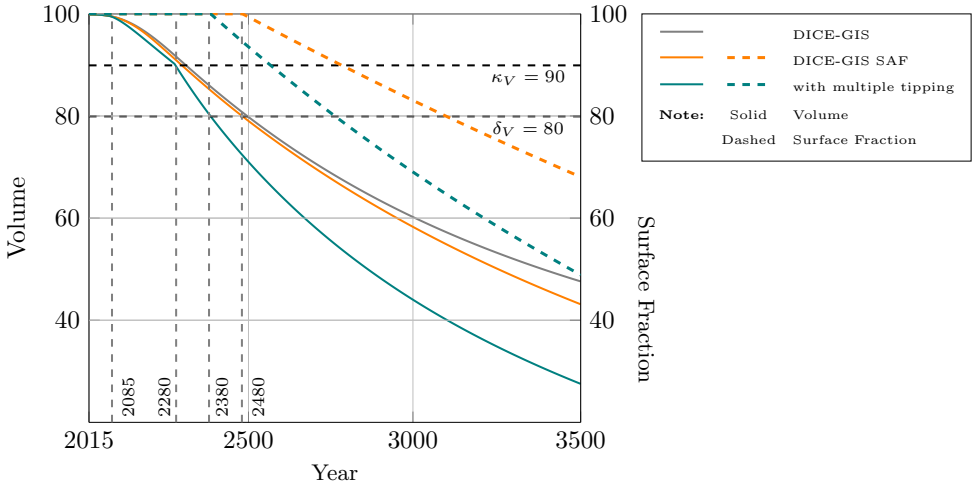

Figure A2: Volume and Surface Fraction

Figure A2 displays the volume of the GIS on the left axis (solid lines) and the surface fraction of the GIS on the right axis (dashed lines) from 2015 to 3500. Compared to the optimal policy, the volume decreases faster and is significantly lower in the long run. Consequently, the surface fraction starts to decrease earlier. Under the non-optimal policy, multiple tipping is reached 100 years in advance in 2280. Moreover, the shrinking of the surface area for DICE-GIS SAF with multiple tipping begins 180 years earlier in 2380. For DICE-GIS SAF, the surface fraction begins to decline in 2480.

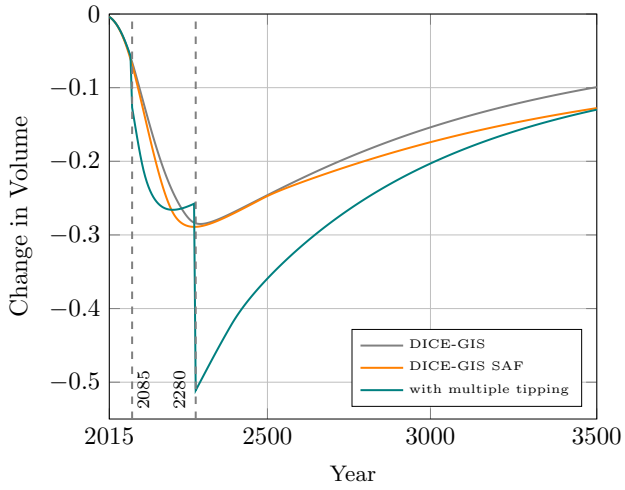

Figure A3: Melt Rate

Figure A3 presents the melt dynamics. In addition to the earlier passing of the tipping thresholds, the melt rate has a higher (more negative) magnitude, which leads to the greater volume loss, see Figure A2. In contrast to the optimal policy, DICE-GIS SAF shows, in the long run, a slightly higher magnitude of the melt rate compared to DICE-GIS.

Temperature Dynamics

Figure A4 shows the temperature increase T_{globe} on the left axis (solid lines) and the feedback parameter on the right axis (dashed lines). The peak increase in temperature is

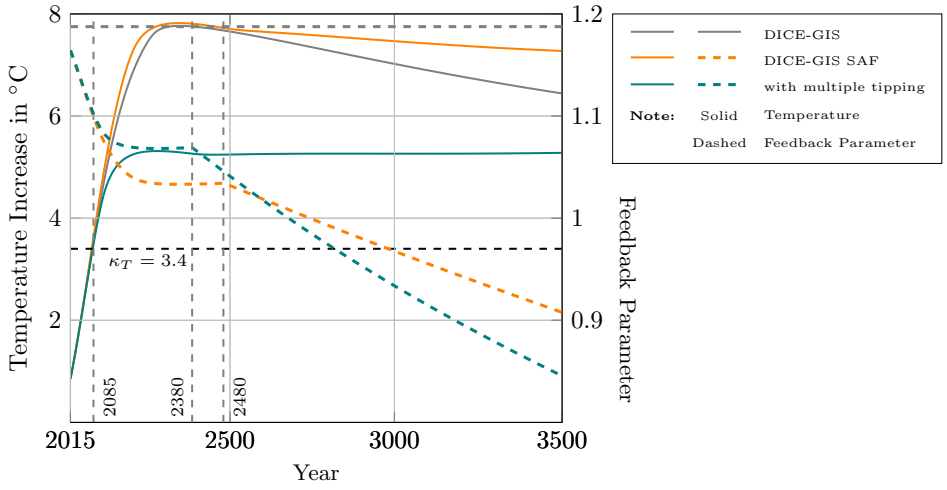

Figure A4: Feedback Parameter

notably higher than under the optimal policy. When accounting for the SAF, the temperature increase shows only a very limited cooling after peaking. Hence, the temperature for DICE-GIS SAF remains at a relatively high level. The threshold κ_T is passed in 2085, 10 years earlier compared to the optimal policy. Surprisingly, the temperature increase is much higher for DICE-GIS SAF than for DICE-GIS SAF with multiple tipping.

In general, the feedback parameter λ_{FB} decreases more than with the optimal policy. After the surface of the GIS starts to decrease in 2380 for DICE-GIS SAF with multiple tipping and in 2480 for DICE-GIS SAF, see also Figure A2, λ_{FB} continues to decline steadily. In contrast to the optimal policy, there is no subsequent increase in the feedback parameter.

D Sensitivity Analysis

The following appendix presents a comprehensive sensitivity analysis for the parameters mentioned in Section 4. The calculations are based on DICE-GIS SAF. Several calculations include tipping. Volume tipping refers to the solely passing of κ_V. While temperature tipping refers to the solely passing of κ_T. Multiple tipping refers to the passing of both thresholds κ_V and κ_T.

Volume and Surface: η

The following analysis is based on DICE-GIS SAF with multiple tipping, because for DICE-GIS SAF, the volume does not fall below $\delta_V = 80$. Figure A5 shows the SCC in dependence to η. Varying η in the range of 0.25 to 0.75 gives no significant change in the SCC in the year 2100. There is an absolute deviation in the peak SCC of -28.20 to 18.55 \$/t CO_2. This gives a relative deviation of -0.65 to 0.40 %.

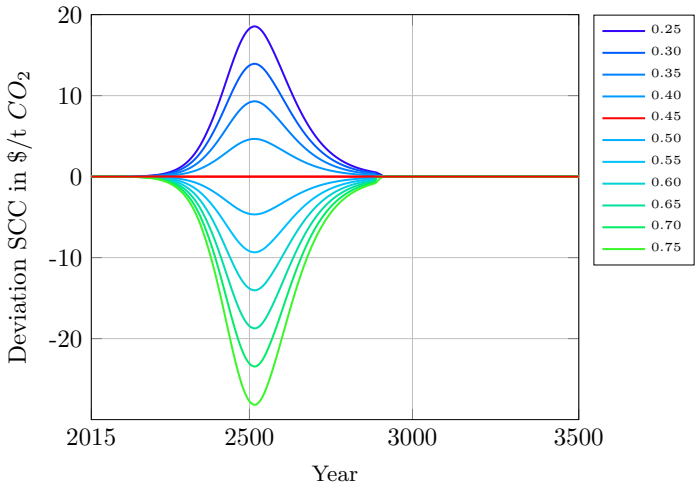

Figure A5: Multiple Tipping - SCC depending on η; Deviation Reference $\eta = 0.45$

Figure A6 displays the volume in dependence to η. The volume in 3500 gives an absolute deviation from -0.94 to 1.40 %p (percentage points).

The higher η, the more convex is the relation between the loss of the volume and the decrease of the surface fraction. Hence, the higher η, the higher is the surface fraction for a given volume. This implies less total albedo loss and thus a lower decrease in the feedback parameter after passing δ_V. Therefore, the temperature increase is negatively correlated to η. Hence, the SCC is relatively lower while the volume is relatively higher.

I conclude that the SCC and the volume are relatively robust to the variation of η.

Volume and Surface: δ_V

The following analysis is based on DICE-GIS SAF with volume tipping. There is no significant deviation in the SCC when varying δ_V from 76 to 85. The absolute deviation of the peak SCC is between -0.2 to 0.7 \$/t CO_2.

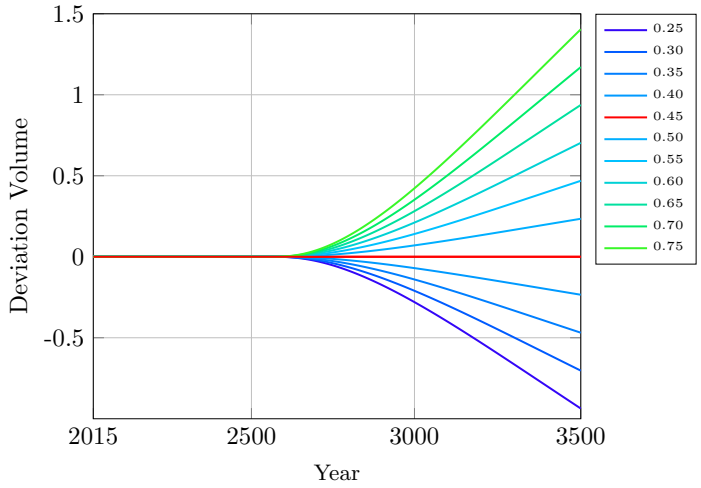

Figure A6: Multiple Tipping - Volume depending on η; Deviation Reference $\eta = 0.45$

Figure A7 shows the impact on the volume. The absolute deviation in 3500 is in the range of -0.26 to 0.09 %p.

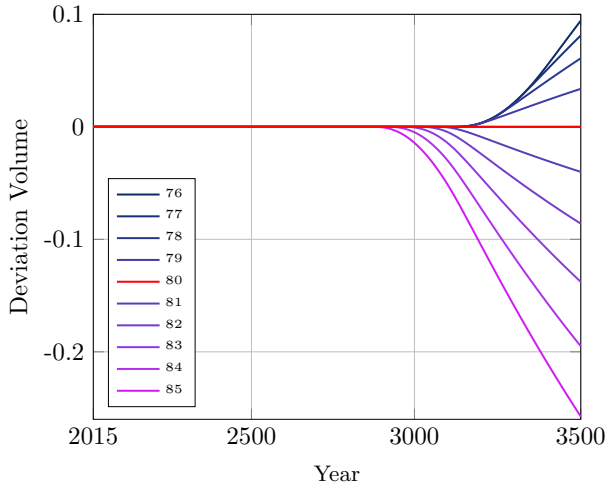

Figure A7: Volume Tipping - Volume depending on δ_V; Deviation Reference $\delta_V = 80$

Note, that the volume starts to deviate earlier for higher values of δ_V, because as the surface fraction declines, there is total albedo loss and the feedback parameter decreases again, see Figure 4. This, in turn, accelerates the temperature increase and promotes the melting of the GIS.

In addition, I vary δ_V from 99.9 to 91 to investigate the impact on DICE-GIS SAF as well. For $\delta_V = 99.9$, the surface fraction starts to decrease almost immediately as the volume melts.

Figure A8 presents the SCC depending on δ_V. The SCC in 2100 shows an absolute deviation of 2.29 \$/t CO_2, or relatively 0.7 %. The peak SCC deviates up to 131.63 \$/t CO_2, or 3.1 %.

Figure A9 shows the volume in dependence to δ_V. The GIS starts to melt comparatively earlier for higher values of δ_V, which reveals a similar pattern as in Figure A7. The volume in 3500 decreases by up to -0.83 %p.

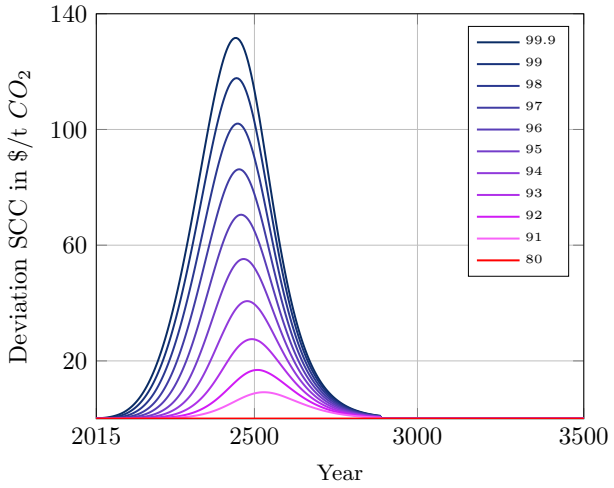

Figure A8: DICE-GIS SAF - SCC depending on δ_V; Deviation Reference $\delta_V = 80$

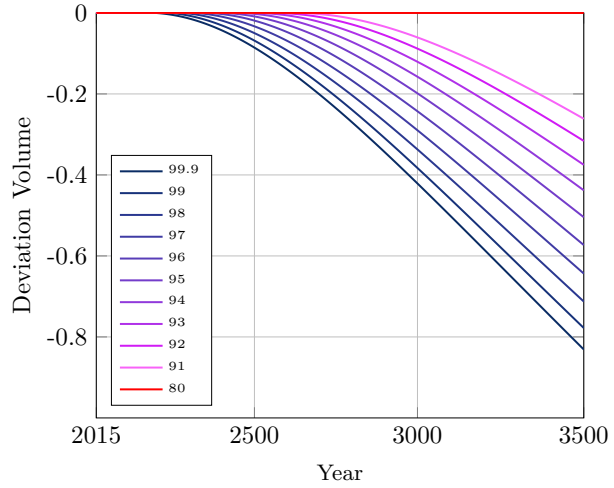

Figure A9: DICE-GIS SAF - Volume depending on δ_V; Deviation Reference $\delta_V = 80$

Consequently, the volume is relatively robust to the variation of δ_V. This holds for DICE-GIS SAF as well as for DICE-GIS SAF with volume tipping. The SCC is sensitive for DICE-GIS SAF under $\delta_V \geq 91$, but not for volume tipping under $75 \leq \delta_V \leq 85$.

SAF: λ_{SAF}

The following analysis is based on DICE-GIS SAF. Figure A10 presents the SCC in dependence to λ_{SAF} in the range of 0.25 to 0.75 (Flanner et al., 2011; Duan et al., 2019; Qu and Hall, 2014; Winton, 2006). The SCC in 2100 differs between -23.83 and 27.47 \$/t CO_2, or -7.5 to 8.5 %. The deviation of the peak SCC is -359.90 to 431.51 \$/t CO_2, or -8.5 to 10.2 %.

Figure A11 shows the influence of the absolute contribution of the SAF to the climate feedback parameter λ_{SAF}. The higher λ_{SAF}, the stronger is the decreasing impact on the global feedback parameter λ_{FB}. Thereby, the course remains almost robust. The feedback parameter in 3500 is in the range of 1.06 to 1.15, a relative deviation of -4.6 to 3.6 %.

I deduce that the SCC and the feedback parameter are sensitive to λ_{SAF}. This under-

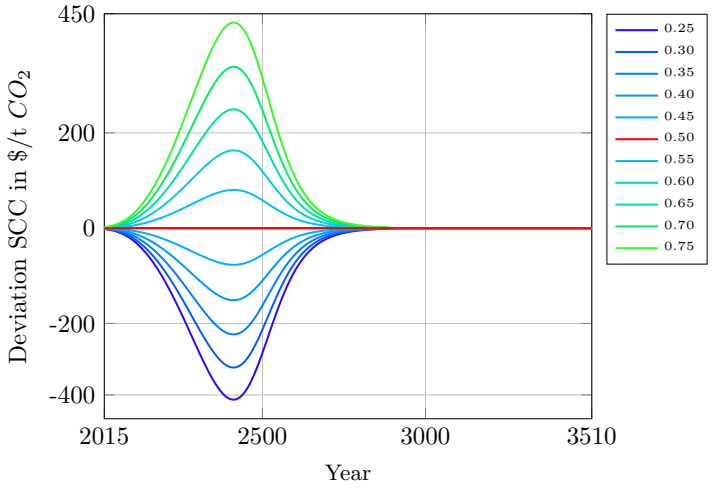

Figure A10: DICE-GIS SAF - SCC depending on λ_{SAF}; Deviation Reference $\lambda_{SAF} = 0.5$

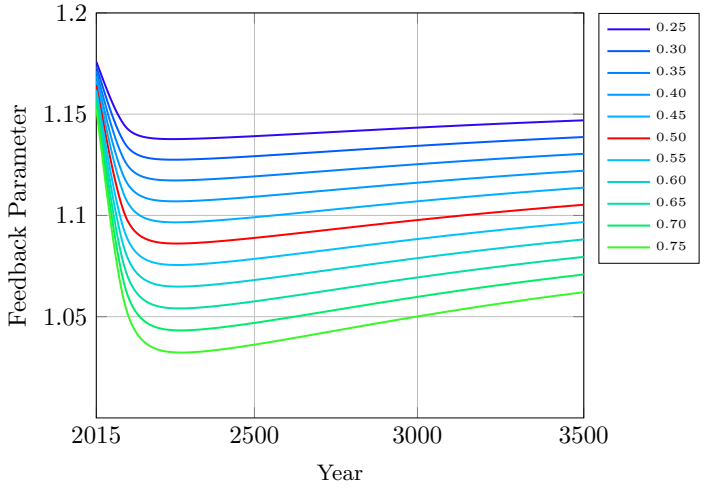

Figure A11: DICE-GIS SAF - λ_{FB} depending on λ_{SAF}; Deviation Reference $\lambda_{SAF} = 0.5$

lines the fact that the SAF plays an important role for the climate and has a significant impact on the SCC.

SAF: γ

The following analysis is based on DICE-GIS SAF. Figure A12 displays the SCC in dependence to γ. The SCC in 2100 varies between -5.89 and 6.09 \$/t CO_2, or -1.8 to 1.9 %. The peak SCC deviates from -89.77 to 93.77 \$/t CO_2, or -2.1 to 2.2 %.

I conclude that the SCC is sensitive to γ, which underlines the impact of the SAF.

Tipping: κ_V

The following analysis is based on DICE-GIS SAF with volume tipping. Figure A13 visualizes the SCC with κ_V varying from 95 to 85. There is no significant impact on the SCC in 2100. The peak SCC deviates in the range of -2.96 to 22.65 \$/t CO_2, or -0.06 to 0.5 %. The volume deviates in the range of -0.05 to 0.06 %p.

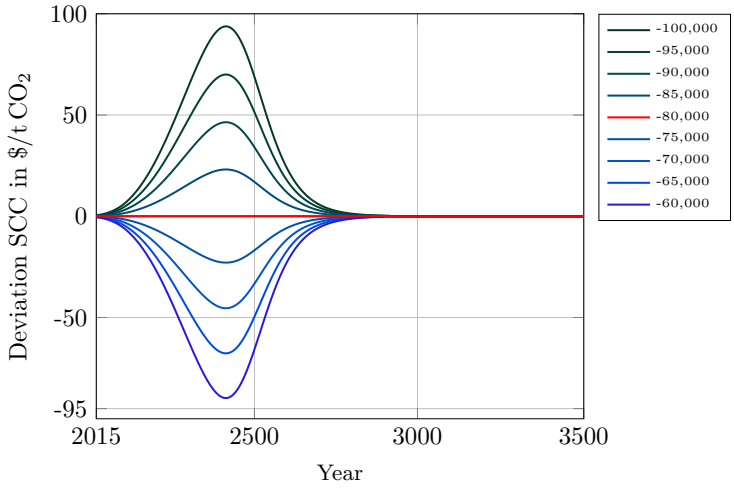

Figure A12: DICE-GIS SAF - SCC depending on γ; Deviation Reference γ = -80,000

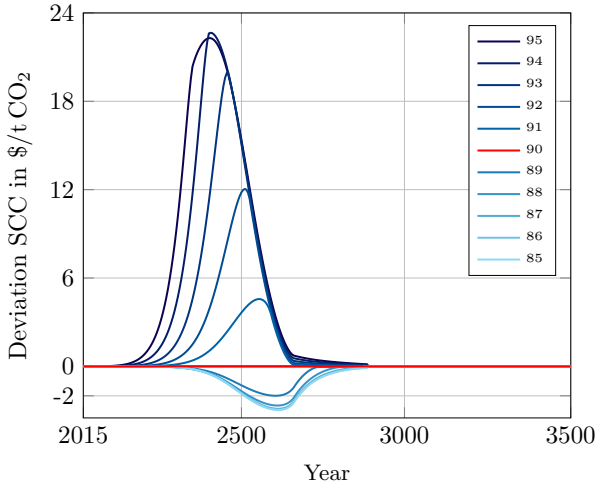

Figure A13: Volume Tipping - SCC depending on κ_V Deviation Reference $\kappa_V = 90$

I derive a limited sensitivity of the SCC to κ_V, while the volume is robust. This is because κ_V is reached very late, see Figure 2.

Tipping: κ_T

The following analysis is based on DICE-GIS SAF with temperature tipping. Figures A14 presents the SCC with κ_T varying from 1.5 to 4.5 °C (IPCC, 2019; Robinson et al., 2012; Ridley et al., 2009). The SCC in 2100 falls by up to -1.52 \$/t CO_2, or 0.04 %. The peak SCC deviates in the range of -20.64 to 0.50 \$/t CO_2, or -0.5 to 0.01 %.

Figure A15 shows the volume depending on κ_T and depicts a similar pattern. The volume is only sensitive for $\kappa_T \geq 3.6$ °C and deviates up to 13.0 %p.

Since the thresholds for $\kappa_T < 3.6$ °C are all reached very early, see Figure 4, temperature tipping starts at about the same time for $1.5 \leq \kappa_T < 3.6$. Therefore, neither the SCC nor the volume shows a significant deviation. For $\kappa_T \geq 3.6$ °C, the SCC and the volume are sensitive as the timing of passing the threshold varies.

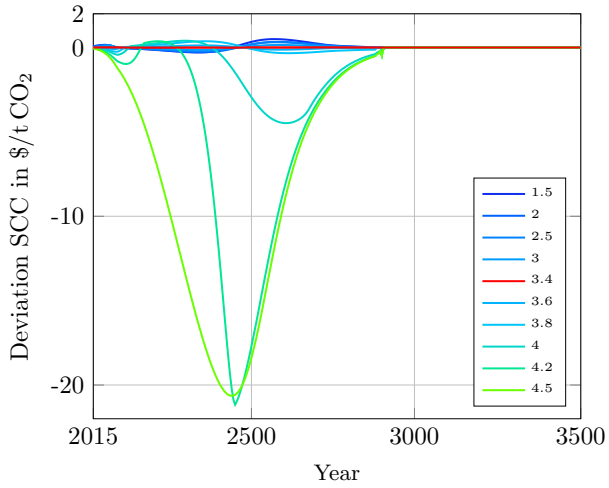

Figure A14: Temperature Tipping - SCC depending on κ_T; Deviation Reference $\kappa_T = 3.4$

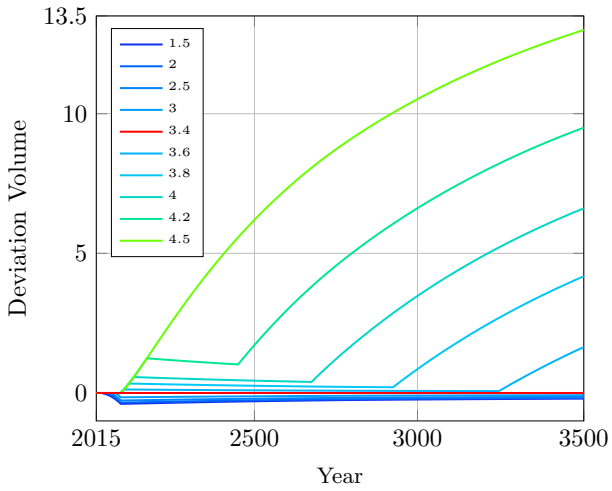

Figure A15: Temperature Tipping - Volume depending on κ_T; Deviation Reference $\kappa_T = 3.4$

Tipping: ρ

The following analysis is based on DICE-GIS SAF with multiple tipping. Figure A16 shows the SCC in dependence to ρ varying from 1.5 to 2.5. There is no significant variation in the SCC in 2100. The peak SCC deviates in the range of -50.23 to 89.60 \$/t CO_2, or by -1.2 to 2.1 %.

The volume deviates in the range of -0.19 to 0.18 %p. I deduce that the SCC and particularly the volume are rather robust to ρ.

Tipping: ψ

The following analysis incorporates DICE-GIS SAF with volume, temperature and multiple tipping. ψ is varied in the range of 1.5 to 4. Figure A17 presents the SCC in variation to ψ.

For DICE-GIS SAF with volume tipping, there is no deviation in 2100. But, the peak SCC varies in the range of -1.37 to 6.66 \$/t CO_2, or -0.03 to 0.16 %. Surprisingly the

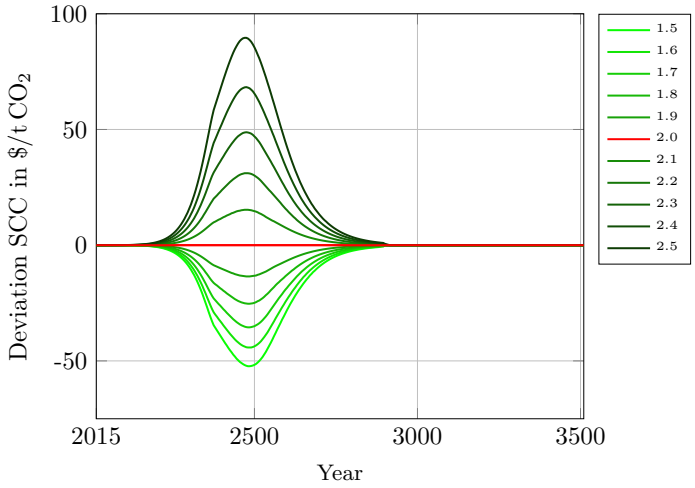

Figure A16: Multiple Tipping - SCC depending on ρ; Deviation Reference $\rho = 2$

SCC for $\psi = 1.75$ initially shows a positive deviation followed by a negative deviation. For DICE-GIS SAF with temperature tipping, the SCC in 2100 varies from -0.75 to 2.95 \$/t CO_2, or -0.02 to 0.09 %. The deviation of the peak SCC is between -10.63 to 171.29 \$/t CO_2, or -0.2 to 4.0 %. For DICE-GIS SAF with multiple tipping and $\psi \leq 3$, the SCC in 2100 varies from -0.79 to 2.27 \$/t CO_2, or -0.2 to 0.7 %. The deviation of the peak SCC is -73.94 to 467.10 \$/t CO_2, or -1.7 to 10.8 %. The SCC is highly sensitive for $\psi > 3$, exploding up to 3.9 million \$/t CO_2.

Figure A18 shows the volume in variation to ψ. Accounting for volume tipping, the volume in 3500 is in the range of 62.16 to 77.54, or -11.92 to 3.46 %p. Accounting for temperature tipping, it is in the range of 48.99 to 74.39, or -19.27 to 6.12 %p. Accounting for multiple tipping, it is in the range of 19.06 to 68.13, or -34.02 to 15.05 %p.

I conclude that, surprisingly, there is only a very small impact for volume tipping. Temperature tipping is quite sensitive to ψ. While accounting for multiple tipping is the most sensitive, because ψ is exponentiated with ρ, see Equation (15).

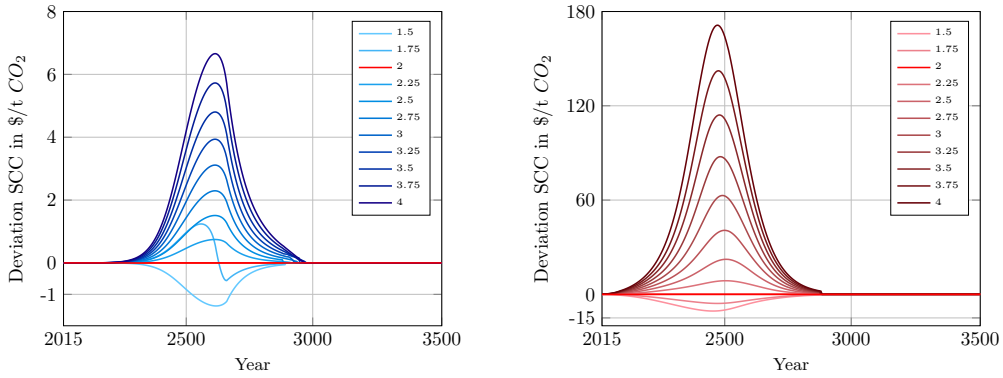

(a) Volume Tipping

(b) Temperature Tipping

(c) Multiple Tipping

(d) Multiple Tipping

Figure A17: SCC depending on ψ; Deviation Reference $\psi = 2$

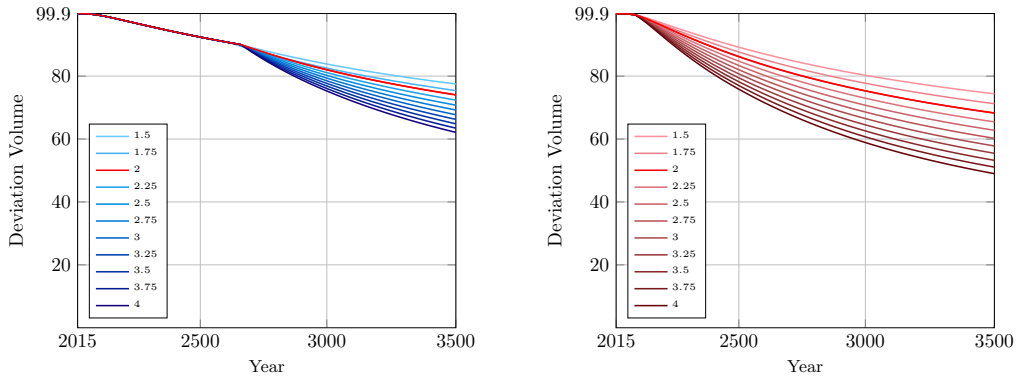

(a) Volume Tipping

(b) Temperature Tipping

(c) Multiple Tipping

Figure A18: Volume depending on ψ; Deviation Reference $\psi = 2$